Aus dem Zentrum Neurologie Neurologische
Universitätsklinik Tübingen
Hertie-Institut für klinische Hirnforschung Abteilung
Neurologie mit Schwerpunkt Epileptologie

Functional studies of mutations in *SCN2A* gene associated with early-onset epilepsy

Dissertation
submitted for a doctoral degree in medicine

at the Faculty of Medicine
of the Eberhard Karls Universität Tübingen

submitted by
Haosi Huang
2019

Dean: **Professor Dr. I. B. Autenrieth**

First reviewer: **Professor Dr. H. Lerche**

Second reviewer: **Professor Dr. B. Antkowiak**

Date of oral examination: **07. 01. 2019**

CONTENT

INDEX OF FIGURES

INDEX OF TABLES

LIST OF ABBREVIATIONS

A1659V	P.Ala1659Val
ACTH	Adrenocorticotropic hormone
AEDs	Antiepileptic drugs
ANOVA	Analysis of Variance
BFNIS	Benign familial neonatal-infantile seizures
C	Capacitance
CNS	Central nervous system
DI-DIV	Domain I-IV
DPBS	Dulbecco's phosphate buffered saline
EE	Epileptic encephalopathy
FBS	Fetal bovine serum
GEFS+	Generalized epilepsy with febrile seizures plus
hNa_V	Human voltage-gated sodium channel
I	Current amplitude
I1640M	P.Ile1640Met
ILAE	International League Against Epilepsy
I_{max}	Maximal current amplitude
K	Slope factor
Na^+	Sodium ions
PBS	Phosphate buffered saline
PNS	Peripheral nervous system
R	Resistance
S1–S6	Segment 1-6
SEM	Standard error of the mean
V	Voltage
$V_{1/2}$	Half-maximum voltage
VGSCs	Voltage-gated sodium channels
WT	Wild-type

1. Introduction

Ion channels control movement of ions, which is recognized as the major mechanism by which cellular electrophysiological homeostasis is maintained. Depending on different gating, there are three types of ion channels (Figure 1). Over one thousand human voltage-gated sodium channel (VGSC) mutations have been identified that are relevant to neurological, skeletal muscle and cardiovascular disorders (Brunklaus et al., 2014). After the patch-clamp technique was developed, it was convenient for researchers to investigate the electrophysiological characteristics of mutations at the cellular level. Recently, many epilepsy-associated ion channel mutations have been reported (Orsini et al., 2017).

Epilepsy, which is a neurological disease and caused by the synchronized abnormal electrical activity of neurons, is characterized by recurrent, transient, and unprovoked seizures. There are 40-50 million people worldwide who have epilepsy (Orsini et al., 2017). With respect to the original site of seizure onset, the newest seizure types are classified into three main categories: (1) focal onset, (2) generalized onset and (3) unknown onset (Fisher, 2017). According to previous studies, genetic factors are an important cause of many epilepsy phenotypes (Kaplan et al., 2016, Orsini et al., 2017).

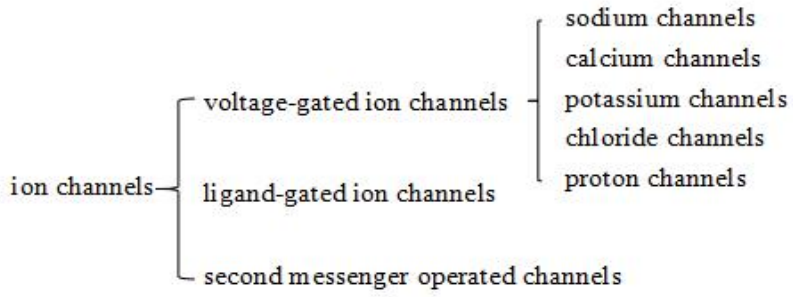

Figure 1: Three types of ion channels.

1.1. VGSCs

VGSCs contain α-subunit and β-subunit (some VGSCs contain two β-subunits). The former forms the channel tunnel and conducts sodium ions (Na^+) passing through the pore (Catterall, 1992, Catterall, 2000, Isom, 2001). The function of β-subunit is to promote membrane localization and modulate the kinetic characteristics of the channels (O'Malley and Isom, 2015).

1.1.1. The family of human VGSC α-subunits

The human VGSCs have nine principal α-subunits—sodium channel protein types 1-9 ($hNa_V1.1$-$hNa_V1.9$) (https://www.ncbi.nlm.nih.gov/protein/) and distribute in different mammals tissues (Brunklaus et al., 2014). VGSC α-subunit genes (*SCN1A*-*SCN6A, SCN8A*-*SCN11A*) encode VGSC α-subunits and locate on the human chromosomes 12q13, 17q23, 2q24 and 3p22, respectively (Meisler et al., 2010). The *SCN1A* through *SCN5A* genes encode $hNa_V1.1$ through $hNa_V1.5$, and the *SCN8A* to *SCN11A* genes encode $hNa_V1.6$ through $hNa_V1.9$. The human VGSCs express in the nervous system, skeletal muscle and cardiac myocytes (Table 1) (Brunklaus et al., 2014). hNa_X which is involved in salt intake has not yet been functionally expressed and fully identified (Watanabe et al., 2000, Shen et al., 2017).

Table 1: Human VGSC α-subunits, revised from (Brunklaus et al., 2014).

p and q: chromosome short and long arm; *SCN1A-6A* and *SCN8A-11A*: VGSC α-subunit gene family; $hNa_V1.1$-1.9 and hNa_X: human VGSC α-subunit proteins.

Gene	Protein	Human chromosome	Channel distribution
SCN1A	$hNa_V1.1$	2q24	central nervous system, cardiac myocytes
SCN2A	$hNa_V1.2$	2q24	central nervous system
SCN3A	$hNa_V1.3$	2q24	central nervous system, cardiac myocytes
SCN4A	$hNa_V1.4$	17q23	skeletal muscle
SCN5A	$hNa_V1.5$	3p22	cardiac myocytes, skeletal muscle, central nervous system
SCN8A	$hNa_V1.6$	12q13	central nervous system, peripheral nervous system
SCN9A	$hNa_V1.7$	2q24	peripheral nervous system
SCN10A	$hNa_V1.8$	3p22	peripheral nervous system
SCN11A	$hNa_V1.9$	3p22	peripheral nervous system
SCN6A	hNa_X	2q21	cardiac myocytes, uterus, skeletal muscle

1.1.2 The structure of VGSC α-subunits

Four domains (DI-DIV) constitute a VGSC α-subunit, and six segments (S1-S6) constitute a domain (Figure 2). All of these four domains are equally required for the sodium channels (Stuhmer et al., 1989). The domains mainly act as voltage-sensing and ion conducting, which control voltage-dependent gating and allow the Na^+ to pass through the membrane (Shen et al., 2017). The channel's voltage sensor locates in S4 transmembrane segment (Stuhmer et al., 1989). A critical hydrophobic amino acid sequence which inactivates the VGSC channels locates in short intracellular loop connecting DIII-IV (Catterall, 2001).

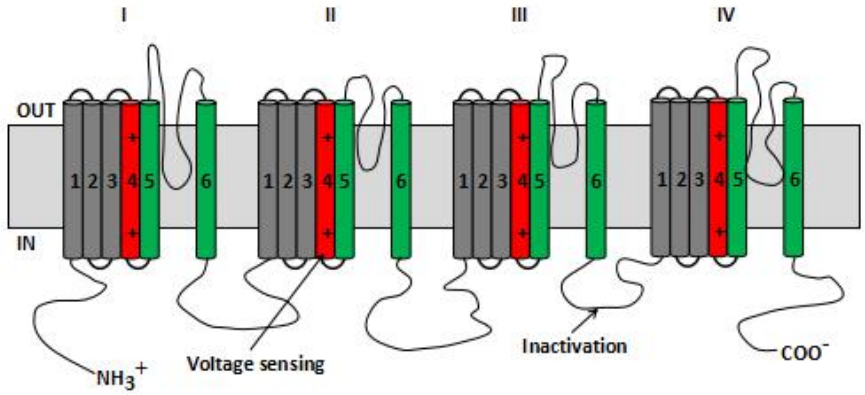

Figure 2: The human VGSC α-subunit.

1-6: segment 1-6; I-IV: domain I-IV; OUT: extracellular membrane; IN: endocellular membrane; +: positive charge; voltage sensing: S4 segments; inactivation: short intracellular loop connecting DIII-IV; NH_3^+: N-terminal; COO^-: C-terminal.

The two-dimensional structure of the VGSC α-subunits are shown spread out and in a row; in actuality, the domains of VGSCs are clustered. With the help of X-ray crystallography, nuclear magnetic resonance and image reconstruction, the channel's space structure was discovered (Catterall, 2001, Sato et al., 2001). The three-dimensional structure provided a feasible way to understand how the channels work.

1.1.3. The function of VGSCs

VGSCs have three different conformational states (Figure 3): (1) the closed state: the membrane is negatively charged inside and positively charged outside with the sodium ions sequestered outside the membrane; (2) the open state: when membrane potential changes, voltage sensor shifts the position within the protein, the activation gate is opened, and sodium ions pass across the sodium channel; and (3) the inactivated state: the inactivation gate is automatically closed, and the sodium ions are sequestered

outside the membrane. When potential changes happen in the membrane, the voltage sensor segment moves toward outside relative to the rest of the protein, and then the activation gate is opened, at which point positively charged sodium ions pass through the sodium channel within several milliseconds. The membrane potential becomes more positively charged. The negatively charged intracellular membrane soon changes its potential to zero or even more positive, this process is called “activation”. According to the activation-inactivation coupling mechanism, the inactivation is related to the activation (Chen et al., 1996). Inactivation gate automatically closes after membrane potential is high enough, and sodium ions cannot pass through the channel (even though activation gate still opens). At this time, the sodium channels are in their inactivation state. Due to lack of positively charged sodium ions passing through the channel, the membrane’s potential cannot maintain original level even decrease. When the membrane’s potential level is low enough, the membrane returns to the resting potential. The inactivation gate is reopened, and the activation gate is closed again, at which point it is ready for another action potential.

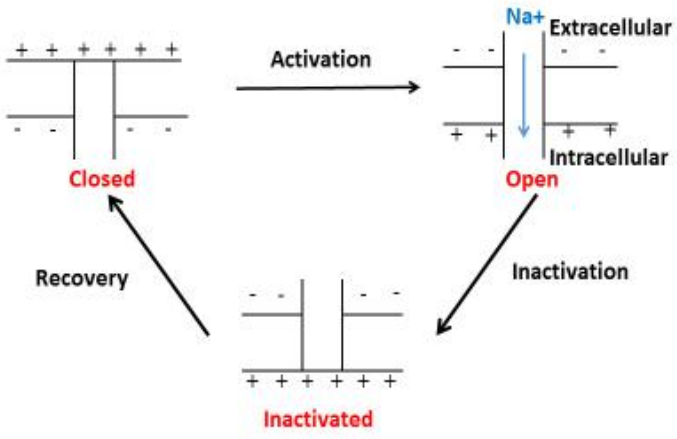

Figure 3: The conformational states of VGSCs.

+: positive charge; -: negative charge.

1.1.4 VGSC β-subunits

In mammals, VGSC β-subunits are of four types, namely subunit β1, β2, β3 and β4. They are encoded by the *SCN1B-SCN4B* genes. The β1-subunit has another splice variant known as β1B-subunit (Isom et al., 1992, Patino and Isom, 2010). Previous studies have shown that each VGSC β-subunit only has one segment with intracellular a C-terminal and extracellular an immunoglobulin-like fold N-terminal (Isom et al., 1995, Catterall, 2014). VGSC β-subunits mainly distribute in neural and cardiac and mutations cause epilepsy and cardiac diseases (O'Malley and Isom, 2015) and modulate channel gating and cell-cell interactions (Catterall, 2000). In heterologous systems, β1 and β2-subunits contribute to extracellular interactions, and β2-subunit increases the sodium current density by enhancing the α-subunit expression in the cell surface (O'Malley and Isom, 2015).

1.2. Epilepsy

Epilepsy is traced back to 2000 B.C., from which time it was discovered in ancient Egyptian medical texts (1700 B.C.) (Magiorkinis et al., 2010). From the time of its first recognition, epilepsy was considered to be associated with the divine malady, evil spirits or demonic possession; Hippocrates, the father of medicine, was the first to doubt its origin and deem brain dysfunction and head injuries as epilepsy's etiology (Magiorkinis et al., 2010). The word "epilepsy" begins with the Greek verb "epilambanein", which means "to seize upon", "to attack" (http://www.epilepsiemuseum.de/alt/introen.html). The neurological study of epilepsy in recent times dates back to the 1860s (Eric R. Kandel, 2000).

Several mutations of the VGSC genes (*SCN1A, SCN2A* and *SCN8A*) have been associated with epilepsies (Scheffer et al., 2017, Orsini et al., 2017).

1.3. *SCN2A* mutations are associated with epilepsy

There are more than 140 epilepsy-associated *SCN2A* mutations. According to the previous studies, *SCN2A* mutations-associated epilepsy phenotype spectrum manifest as

benign familial neonatal-infantile seizures (BFNIS), generalized epilepsy with febrile seizures plus (GEFS+) and epileptic encephalopathies (EE) (Lerche et al., 2013, Brunklaus et al., 2014, Howell et al., 2015). Inherited *SCN2A* mutations contribute to milder phenotypes such as BFNIS, usually *de novo SCN2A* mutations cause severe EE (Shi et al., 2012, Brunklaus et al., 2014). *SCN2A* mutations were functionally characterized as either enhance or decrease the channel function (Liao et al., 2010a, Liao et al., 2010b, Schwarz et al., 2016, Wolff et al., 2017).

1.3.1. BFNIS

The onset of afebrile generalized seizures in the neonatal period is the main clinical feature of BFNIS; other characteristics of this disease are responding well to anticonvulsants and self-limiting (Striano et al., 2006). $Na_V1.6$ replaces $Na_V1.2$ during development in axon initial segments (Liao et al., 2010b). This could explain why BFNIS is a self-limiting disease. According to the previous studies, most *SCN2A*-related BFNIS cases tend to heritable missense mutations (Gardiner, 2006, Shi et al., 2012, Yallapu et al., 2012).

1.3.2. GEFS+

Scheffer and Berkovic firstly described GEFS+ in 1997, and it appears various seizure types and responds to most of antiepileptic drugs (AEDs), and these seizures stop spontaneously in some cases (Ito et al., 2002, Kamiya et al., 2004). Not only *SCN2A* variants but also mutations of *SCN1B* and *SCN1A* are related to GEFS+ (Lossin et al., 2002). Proprietorial *SCN2A* mutations associated with the GEFS+ cases involve inherited missense mutations (Shi et al., 2012).

1.3.3. EE

The concept of EE was accepted by International League Against Epilepsy (ILAE) in 2001. EE are severe epileptic syndromes, and most of the cases are resistant to AED treatment. Their clinical features manifest as generalized or focal seizures, cognitive dysfunction or decline, behavioral and or motor slowing or regression, and developmental regression; the clinical features may evolve from one type to another during the maturation process (Covanis, 2012). Some cases show persistent, severe electroencephalography abnormalities. EE affect cerebral function and usually occur in the early of life (Engel and International League Against, 2001, Engel, 2006, Covanis, 2012). EE mainly include eight kinds of syndromes (Table 2) (Covanis, 2012). Some human VGSC mutations have been reported that related to EE (Lerche et al., 2013, Gokben et al., 2017). According to previously reported cases, some mutations of *SCN2A* are related to early-onset EE (Syrbe et al., 2016, Wolff et al., 2017). Not all phenotypes fit into one category and therefore unspecific EE is another category which can occur at any age (Wolff et al., 2017). Most of these *SCN2A* mutations related to EE are *de novo* missense or truncating (Brunklaus et al., 2014).

Table 2: Epileptic encephalopathies (Covanis, 2012).

CSWS: Epileptic encephalopathy with continuous spike-and-wave during sleep; EE: Epileptic encephalopathies; EME: Early myoclonic encephalopathy; EIMFS: Epilepsy of infancy with migrating focal seizures; DS: Dravet syndrome.

period	EE
≤ 28 day	EME Ohtahara syndrome
≤ 1 year	EIMFS West syndrome DS Myoclonic encephalopathy in nonprogressive disorders
Before adolescence	CSWS Lennox-Gastaut syndrome

1.3.4. Ohtahara syndrome

Ohtahara syndrome appears in the early infancy period (usually younger than 3 months after birth) (Khan and Al Baradie, 2012). The main seizure types of Ohtahara syndrome include tonic spasms, focal seizures and rarely massive myoclonus (Covanis, 2012). Structural CNS abnormalities and, in particular, malformations of brain development are the main etiologies of Ohtahara syndrome (Covanis, 2012). Commonly, cases progress to West syndrome or Lennox-Gastaut syndrome (Khan and Al Baradie, 2012). Cases are highly resistant to AEDs. However, a recent report showed that adrenocorticotropic hormone (ACTH) can be effective in some patients (Wilmshurst et al., 2015). Mutations in *SCN2A,* which are relevant to Ohtahara syndrome, are usually *de novo* (Wolff et al., 2017).

1.3.5. EIMFS

EIMFS, which is an uncommon, AED-resistant and cryptogenic infancy EE (Coppola et al., 1995, Covanis, 2012, Khan and Al Baradie, 2012). The characteristic seizures of EIMFS are focal motor seizures which “migrate”, i.e. occur in different regions of the cortex, and frequent secondary generalization (Covanis, 2012). Recent studies have reported that, with vigabatrin and phenytoin treatment, some *SCN2A*-associated cases can become seizure-free (Wolff et al., 2017).

1.3.6. DS

DS usually appears during the infancy period and was first reported by Dravet in 1978; it responds incompletely to AEDs (http://www.omim.org/). Dravet syndrome cases have mainly been associated with *SCN1A* mutations (Lerche et al., 2013, Brunklaus and Zuberi, 2014, Catterall, 2014, Poryo et al., 2017). Mutations of *SCN2A* relevant to DS are usually missense (Shi et al., 2009).

1.3.7. West syndrome

West syndrome appears in the infantile period (usually, 3-6 months of age) with the clinical features of hypsarrhythmia on electroencephalography and developmental deterioration (Covanis, 2012, Khan and Al Baradie, 2012). Most cases of West syndrome are symptomatic; the second-most common form is cryptogenic. The etiology of symptomatic West syndrome includes underlying structural causes and metabolic and mitochondrial causes. *SCN1A* and *SCN2A* are the most frequently observed genes accounting for West syndrome (Epi4k et al., 2013). According to recent studies, all *SCN2A*-related West syndromes showed pharmacoresistance (Wolff et al., 2017). However, some previous researches have shown it might respond well to the ACTH and topiramate (Samanta and Ramakrishnaiah, 2015).

1.3.8. Intractable childhood epilepsy

Children who have one or more uncontrolled seizure in one month at least 2 years and who have used at least three AEDs monotherapy or in drug combination during this time are described as having intractable childhood epilepsy. Although most mutations of drug-resistant epilepsy locate in *SCN1A*, some *de novo SCN2A* mutations are responsible for sporadic intractable epilepsy (Ogiwara et al., 2009, Wang et al., 2012, Wolff et al., 2017).

1.4. Aim

This thesis aimed to investigate the features resulting from A1659V (p.Ala1659Val) and I1640M (p.Ile1640Met) mutations of the *SCN2A* gene making use of the patch-clamp technique in tsA201 cells co-expressed with *SCN2A* (wild-type (WT) or mutation), together with the $h\beta_1$ and $h\beta_2$-subunit.

2. Materials and methods

2.1. Electrophysiological experiment

2.1.1. Mutagenesis

It was performed by co-workers in the laboratory of Laurence Colleaux, Molecular and Pathophysiological Bases of Cognitive Disorders laboratory, Paris Descartes-Sorbonne Paris Cité University, Imagine Institute, Necker-Enfants Malades Hospital in France.

2.1.2. Obtaining plasmid DNA

According to the Genopure Plasmid MaxiPrep Kit (Roche) protocol plasmid DNA was obtained. The purity plasmid DNA concentration and the ratio of A260/280 were checked by using spectrophotometer (Nano Drop®, Biotechnologie GmbH, USA).

2.1.3. Cell culture

A range of mammalian cell lines can be used for *in vitro* studies of protein functions (Venkatachalan et al., 2007). The tsA201 cells were derived from a human kidney cell line. The tsA201 cells are an ideal model for expressing heterologous VGSCs because there are only a small number of endogenous VGSCs in it. In this thesis, the *SCN2A* WT or mutation alpha subunit together with hβ_1 and hβ_2-subunit were co-expressed in the tsA201 cells for electrophysiological characteristics analyzing.

The procedure of the cell culture was performed as follows: Before initiating a cell subculture, the cell growth medium (Table 3) was put in a 37 °C water bath for 15 minutes. A bench (Unity™ Labservices, Germany) was sterilized by UV lamps for 10-20 minutes, where the cell subculture was subsequently performed. A new T-75 flask (Falcon®, USA) was filled with 10 ml fresh cell growth medium. The cells were taken out of the incubator (Integra Bioscience or Greiner, Frickenhausen, Germany) and put on the bench. The old cell growth medium was discarded and replaced by 10 ml fresh cell growth medium with a 10-ml pipette (Serologische, France) softly blown up and

down to separate the adherent cells. The final density of cells for a subculture was approximately 1000,000 cells/ml. The cells grew in a 5 % CO_2 incubator at 37 °C. The cell line was subcultured once a week. Cells were used for transfection until passage 30.

Table 3: The composition of cell growth medium.

Cell growth medium	Products information
1 % L-glutamine	Biochrom GmbH, Deutschland
10 % fetal bovine serum	PAN-Biotech GmbH, Deutschland
89 % Dulbecco's Modified Eagle Medium	Life Technologies, USA

2.1.4. Transfection

The tsA201 cells were split into 35-mm petri dishes a day before transfection. The tsA201 cells used for transfection was approximately 700,000 cells/dish. The *SCN2A* WT or mutant plasmid DNA together with hβ_1-GFP and hβ_2-CD8 plasmid DNA were always transiently co-transfected into tsA201 cells.

Two hundred and fifty microliters of Opti-MEM® I (1×) reduced serum medium (Gibco® by life technologies™, UK) and 7.5 microliters Mirus (TransIT®-LT1 Transfection Reagent, USA) were added into a 1.5-ml tube. After an incubation time of five minutes, a total of 2.4 μg DNA was added into each tube, with the molar ratio of human VGSC α-subunit (*SCN2A* WT or mutation): hβ_1-subunit: hβ_2-subunit = 1: 1: 1 (human VGSC α-subunit 2.0 μg, hβ_1-subunit and hβ_2-subunit were each 0.2 μg). The mixture was sufficiently mixed by vibrating the tube wall and setting for 20 minutes. Then, the mixture was added to each dish, which was filled with tsA201 cells. These transfected cells were finally cultured in a 37 °C incubator for 24 hours. Twenty-four hours later, each dish of the transfected cells was split into several 35-mm petri dishes (usually 5 petri dishes). The cells were set in a 37 °C incubator for 2-3 hours before recording.

Before electrophysiology recording, the old transfection growth medium was discarded and replaced by 2 ml $DPBS^{++}$-CD8 solution (a mixture of 50 ml PBS containing Ca^{2+} and Mg^{2+} and 50 µl Dynabeads CD8), and the cells were exposed to room temperature for 2-3 minutes. Then, 2 ml bath solution took place of the $DPBS^{++}$-CD8 solution in the dish with transfected tsA201 cells. The transfected tsA201 cells were confirmed by fluorescent microscopy. Only cells both with microbeads and green fluorescence were used for electrophysiology recording (Figure 4).

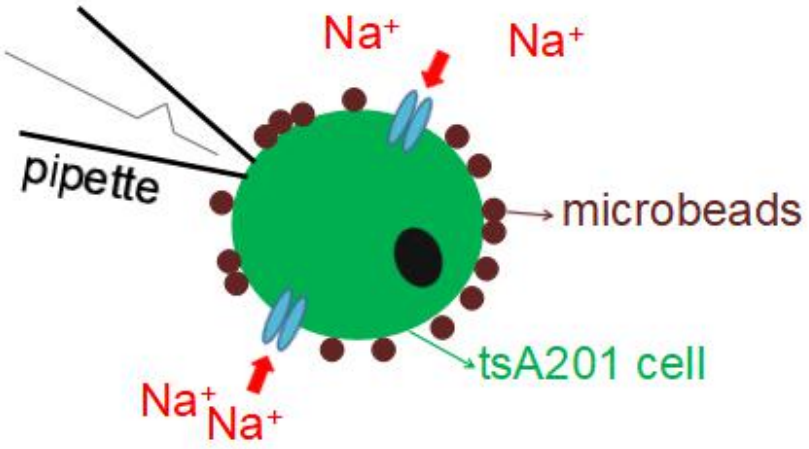

Figure 4: The transfected tsA201 cell used for electrophysiology recording (both with microbeads and green fluorescence under the microscope).

2.2. Electrophysiology technique

2.2.1. Introduction for electrophysiological technology

With patch-clamp electrophysiology coming out at the end of the 1970s, patch-clamp has gradually become the main tool for ion channel electrophysiological characteristics analyzing.

The patch-clamp technique was divided into two types according to control current or potential. Current-clamp consists of applying a current and measuring the changes in membrane potential caused by the applied current; in contrast, the voltage-clamp technique is described as controlling the membrane potential and measuring the transmembrane current required to maintain that potential (Molleman, 2002). The voltage-clamp technique was used in this experiment.

The patch-clamp technique has four configurations (Figure 5) (Molleman, 2002). When the micropipette attaches the cell membrane, the cell-attached patch mode is formed. When the attached membrane is broken, the whole-cell patch-clamp is obtained. Our study used whole-cell patch-clamp configuration for the electrophysiological analysis.

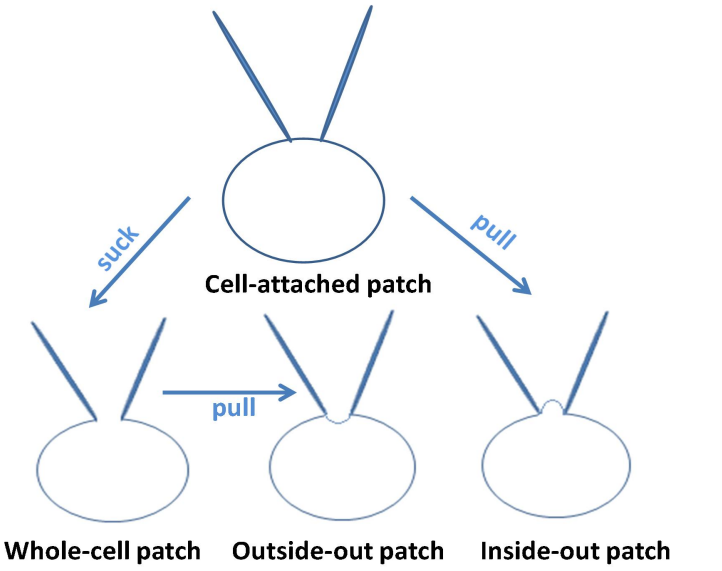

Figure 5: Patch-clamp configurations.

2.2.2. Platform

The basic elements of a setup consisted of an anti-vibration table on which were the inverted microscope (Axio-Vert.A1, Zeiss) and the motorized micromanipulator (LN Unit Junior, Germany). A faraday cage was used to prevent electromagnetic interference. An Axopatch 200B amplifier (Molecular Devices, USA), a Digidata1320A digitizer, a computer, pCLAMP 8 software and a 35-mm petri dish recording chamber were used for recording (Figure 6).

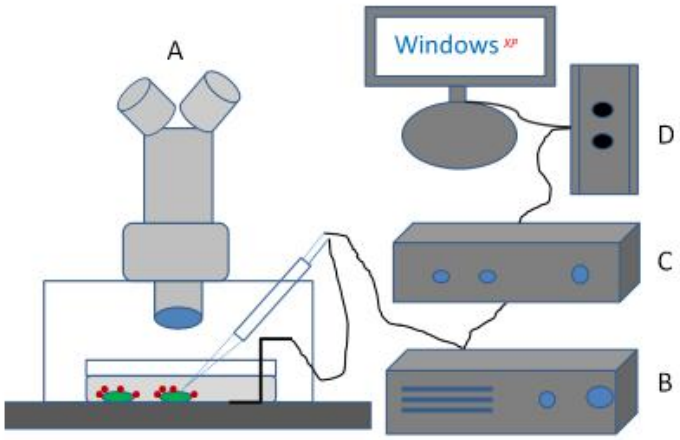

Figure 6: The main basic elements of the patch-clamp setup.

A: Whole-cell voltage-clamp recording on the anti-vibration table. B: Patch-clamp amplifier received the signal then amplified and filtered it. C: Digitizer digitized the output from the amplifier and signals was converted from analog to digital format and stored it on a computer. D: Computer running pCLAMP 8 data acquisition software.

2.2.3. Recording procedure

The experiment was performed at 21-23 ℃. Transiently transfected *SCN2A* WT and mutant tsA201 cells were always recorded on the same day.

Before starting electrophysiology recording, all the setup were switched on and the bath solution and pipette solution were heated in a 37 ℃ water bath after taking out of the

cold room. Only cells which with both microbeads and green fluorescence were used for recording. Before the pipette touched the bath solution, a positive pressure was given by using a syringe (BD, Franklin Lakes, USA). The electrode was located in a borosilicate glass micropipette with resistance between 1-2 MΩ when touched bath solution. Releasing this positive pressure after a tight seal. A gigaohm seal (resistance higher than 1 GΩ) was formed with a gentle suction (by a syringe). Seal quality could be improved by changing the voltage-clamp to a negative potential closed to the resting potential (-70 mV) to the pipette. After this step, a light and short suction pulse was applied by using a 30-ml syringe to break through the membrane. Once the membrane was broken, the whole-cell configuration was obtained. The compensation of the capacitance and series resistance was adjusted up to 90 %. Then the pipette solution and the cytoplasm mixed. Thus, the whole-cell configuration equivalent circuit was obtained (Figure 7). 10 minutes later, when it reached a steady-state, and the experiment could begin to be recorded. It was necessary to frequently check for the cell and micropipette while recording, in case of micropipette drift. The standard parameters of each patched cell were written down on a laboratory notebook. The parameters were as follows: pipette resistance, seal resistance, series resistance (access resistance plus pipette resistance), cells capacitance and percent series resistance compensation.

The whole-cell sodium currents between 1-10 nA were chosen for data analyzing. Compensating the series resistance up to 90 % and controlling the maximal voltage error $\leqslant$5 mV.

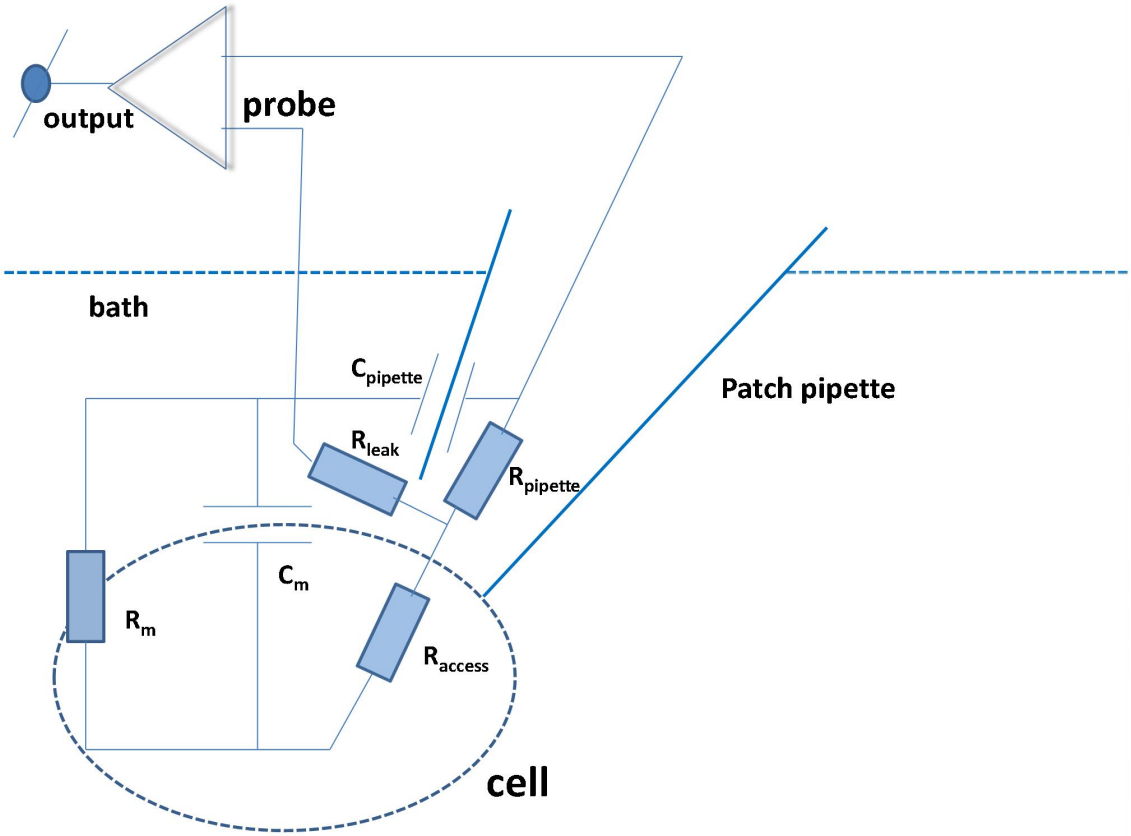

Figure 7: The whole-cell voltage-clamp equivalent circuit (Molleman, 2002).

R_{access}: access resistance, $R_{pipette}$: pipette resistance, R_{leak}: leak resistance, R_m: membrane resistance, $C_{pipette}$: pipette capacitance, C_m: membrane capacitance. The series circuit consists of the $R_{pipette}$, the R_{access} and the R_m, the R_{leak} parallel to the circuit. The series resistance is equal to the sum of $R_{pipette}$ and R_{access}.

2.2.4. Micropipettes

Borosilicate glass micropipettes were pulled from a Sutter P97 Puller. The micropipettes were made and used immediately (usually within 24 hours) to avoid pollution and ensure sealing quality. Pipettes resistance varied from 1 to 2 MΩ.

2.2.5. Electrophysiology recording from transfected tsA201 cells

The electrophysiological experiments were under the condition of room temperature (21-23 ℃). The transfected tsA201 cells were incubated with 2 ml $DPBS^{++}$-CD8

solution (as mentioned earlier) for 2-3 minutes before recording. Then the transfected cells cultured in the bath solution were confirmed by fluorescent microscopy with a 35-mm petri cell culture dish as the recording chamber. The cells that bounded microbeads and showed green fluorescence were chosen for recordings. The recorded sodium currents ranging from 1 to 10 nA were chosen for evaluation.

2.2.6. The solution for electrophysiology recordings

For electrophysiology recordings, the following pipette and bath solutions were used (in mM), as published previously (Schwarz et al., 2016) (Table 4):

Table 4: Electrophysiology recording solution.

The intracellular solution (pipette solution), the extracellular solution (bath solution).

Solution	Composition						PH	Osmotic pressure (mOsm)
Intracellular (in mM)	CsF 130	$MgCl_2$ 2	EGTA 5	HEPES 10	NaCl 5	-	7.4 CsOH adjusted	290
Extracellular (in mM)	$CaCl_2$ 2	Dextrose 4	HEPES 5	$MgCl_2$ 1	NaCl 140	KCl 4	7.4 NaOH adjusted	300

2.3. Whole-cell voltage-clamp protocols

2.3.1. Activation

To study activation a stepwise protocol was used. The cells were progressively depolarized to test pulses between -105 to +97.5 mV with 7.5 mV increments at a -120 mV command pulse. The parameter of the activation curve was fit with Boltzmann equation:

$$\frac{g}{g_{max}}(V) = \frac{1}{1+\exp\left[\left(V - V_{½}\right)/K_V\right]}$$

g : conductance and equal to $I/(V - V_{rev})$, V : given pulse, V_{rec} : reversal potential, g_{max} : maximum conductance, $V_{½}$: half-maximum activation voltage, K_V : slope factor.

2.3.2. Fast inactivation

It was determined by holding and test pulse procedure. The membrane was depolarized for 300 ms at various prepulses (between -170 and -20 mV, with 7.5 mV increments) and finally to -20 mV test pulse.

The parameter inactivation curve was fit to Boltzmann equation:

$$\frac{I}{I_{max}}(V) = \frac{1}{1+\exp\left[\left(V - V_{½}\right)/K_V\right]}$$

(I_{max}) I : (maximum) current amplitude, V : voltage of conditioning pulse, $V_{½}$: half-maximum inactivation voltage, K_V : slope factor.

2.3.3. The time constant of fast inactivation and persistent current

The current decay during activating depolarizations can be described as a fast inactivation time constant. The data were fit to an exponential function of second-order:

$$I(t) = A_f \exp[-(t - t_0)\tau_f] + A_S \exp[-(t - t_0)\tau_S] + C$$

I : current, A_f and A_s : fast and slow amplitude, τ_f and τ_s : fast and slow time constant, t_0 : delay, C : constant.

To determine the persistent current, a protocol depolarizing from -80 to +10 mV with 10 mV increments within 95 ms at a -120 mV command pulse was used.

2.3.4. Recovery from fast inactivation

Firstly, all the sodium channels were inactivated to depolarize all cells to -20 mV at a -120 mV command pulse within 100 ms. Then repolarized to -80, -100 and -120 mV, respectively. Subsequently, the second depolarization to -20 mV was performed at increasing intervals, resulting in increasing amplitude and reflecting the characteristic of recovery associated with fast inactivation.

The data were fit with an exponential function of second-order:

$$I(t) = A_1\left(1 - \exp\left[-(t - t_0)/\tau_1\right]\right) + A_2\left(1 - \exp\left[-\left(t/\tau_2\right)\right]\right) + C$$

A_1 and A_2 : amplitude 1 and 2, τ_1 and τ_2 : time constant 1 and 2, t_0 : delay, C : offset.

2.4. Data and statistical analysis

Originally recorded traces were copied from patch-clamp setup computer and presented to another computer off-line with Clampfit 10.4. Original data were conserved in Microsoft Excel and final graphics were acquired with Origin 6.1 software, statistical tests were run with SigmaPlot 14.0. All data were checked for normality testing (Shapiro-Wilk test) and equal variance testing (Brown-Forsythe). Post Hoc test was used for the power test. One way ANOVA was analyzed distributing normally with equal variance data; Kruskal-Wallis ANOVA on ranks was used for data that were non-normal or unequal variance. Mean ± SEM (standard errors of the mean) was used as data representation. Significant difference levels were described as: p-value<0.05, <0.01 and <0.001. One way ANOVA test was marked as $^{\#}$, $^{\#\#}$ and $^{\#\#\#}$, meaning p value <0.05, <0.01 and <0.001; Dunnet's test was used to correct multiple comparisons between WT and mutation groups; Kruskal-Wallis ANOVA on ranks test was marked as $^{※}$, $^{※※}$ and $^{※※※}$, meaning p-value <0.05, <0.01 and <0.001; Dunn's test was used to correct multiple comparisons between WT and mutation groups.

3. Results

The clinical investigations of the p.Ile1640Met (I1640M) and p.Ala1659Val (A1659V) mutations were performed by our collaborators Prof. Rima Nabbout and her team in Reference Centre for Rare Epilepsies, Department of Pediatric Neurology, Necker-Enfants Malades Hospital, Imagine Institute, Paris Descartes University, APHP & Inserm U1129, Paris, France.

The A1659V and I1640M mutations relate to patients with severe forms of neonatal-onset epilepsy. Both had a similar neonatal electro-clinical phenotype.

3.1. The location of the I1640M and A1659V mutations of *SCN2A* relate to neonatal-onset epilepsy in the hNa$_v$1.2

In this experiment, there are two neonatal-onset epilepsy-associated *SCN2A* mutations (A1659V and I1640M), which locate very close to each other in DIV. As it is shown in Figure 8, the position of the I1640M mutation is in the DIV-S4, whereas the A1659V mutation situates in the intracellular loop of the DIV-S4-S5. The mutations together with amino acid sequences of surrounding mutations are highly conservative during evolution among different species (Table 5).

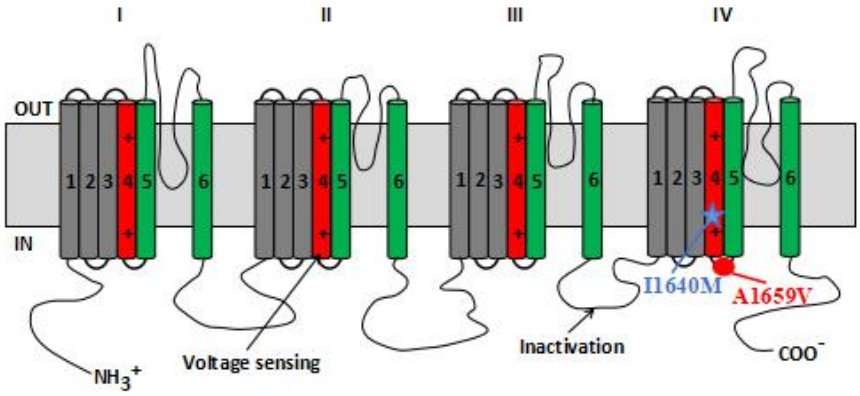

Figure 8: The location of the I1640M and A1659V mutations of *SCN2A* associated with neonatal-onset epilepsy in the hNa$_V$1.2.

The position of I1640M mutation is DIV-S4 and A1659V mutation is DIV-S4-S5. 1-6: segment 1-6; I-IV: domain I-IV; OUT: extracellular membrane; IN: endocellular membrane; +: positive charge; voltage sensing: S4 segments; inactivation: short intracellular loop connecting DIII-IV; NH_3^+: N-terminal; COO^-: C-terminal.

Table 5: The surrounding amino acid sequences of I1640M and A1659V mutations in different species.

Species	I1640M	A1659V
Homo	I L R L **I** K G A K	M S L P **A** L F N I
H.s. (mutated)	I L R L **M** K G A K	M S L P **V** L F N I
Pan troglodytes	I L R L **I** K G A K	M S L P **A** L F N I
Macaca mulatta	I L R L **I** K G A K	M S L P **A** L F N I
Mus musculus	I L R L **I** K G A K	M S L P **A** L F N I
Danio rerio	I L R L **I** K G A K	M S L P **A** L F N I

As mentioned before, the function of the S4 segment is important and as the voltage sensing of VGSCs, and the intracellular linker of S4-S5 directly connects to the S4 segment. These two mutations are located in highly conservative and functionally critical regions. Either I1640M or A1659V mutant, together with two auxiliary $h\beta_1$ and $h\beta_2$-subunit genes, were co-transfected into the tsA201 cells for electrophysiological analyses.

3.2. Prediction functional damage with both mutations using PolyPhen-2 software

The two mutants were predicted by using PolyPhen-2 software, yielding scores of 1.000 (A1659V) and 0.993 (I1640M), respectively (Figure 9). The predictions suggested that both mutations were highly likely to be damaging to $hNa_V1.2$.

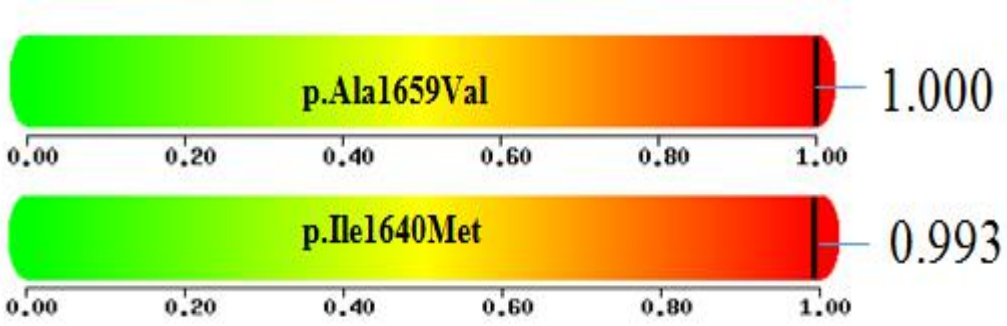

Figure 9: PolyPhen-2 software predicted scores.

These two mutations were predicted to likely be damaging, with scores of 1.000 (the A1659V mutation) and 0.993 (the I1640M mutation).

As mentioned above, according to the particular location and the PolyPhen-2 prediction scores of these two mutations, we stated a hypothesis that these two variations could change the functional characteristics of $hNa_V1.2$. To detect the functional defects caused by these two mutations, we analyzed the kinetics and voltage-dependent characteristics of $hNa_V1.2$ in the transfected tsA201 cells.

3.3. The functional characteristics of WT and mutations in hNa$_V$1.2

To test the hypothesis that functional defects of hNa$_V$1.2 could be caused by the A1659V and I1640M mutations, The *SCN2A* WT or mutant plasmid DNA together with hβ_1-GFP and hβ_2-CD8 plasmid DNA were transiently co-transfected into tsA201 cells. To analyze the electrophysiological features of hNa$_V$1.2 making use of the whole-cell voltage-clamp technique. The detailed functional features of hNa$_V$1.2 were analyzed by current density, persistent currents, activation and fast inactivation curves, the time constants of fast inactivation and recovery from fast inactivation.

3.3.1. hNa$_V$1.2 whole-cell Na^+ current traces

hNa$_V$1.2 whole-cell Na^+ current traces were shown in Figure 10 below. In this thesis, the peak whole-cell Na^+ currents ranging from 1 nA to 10 nA were ultimately chosen for electrophysiological analyses.

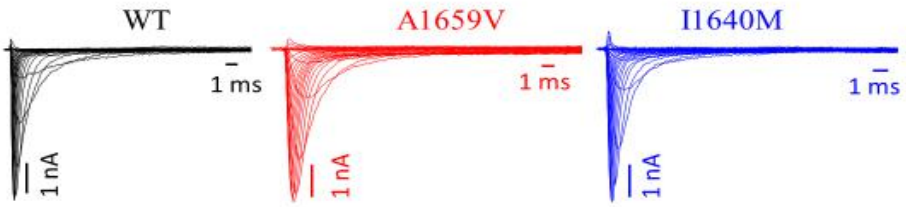

Figure 10: **Representative whole-cell Na^+ current traces.**

Black traces: WT; red traces: A1659V mutation; blue traces: I1640M mutation.

3.3.2. Current density

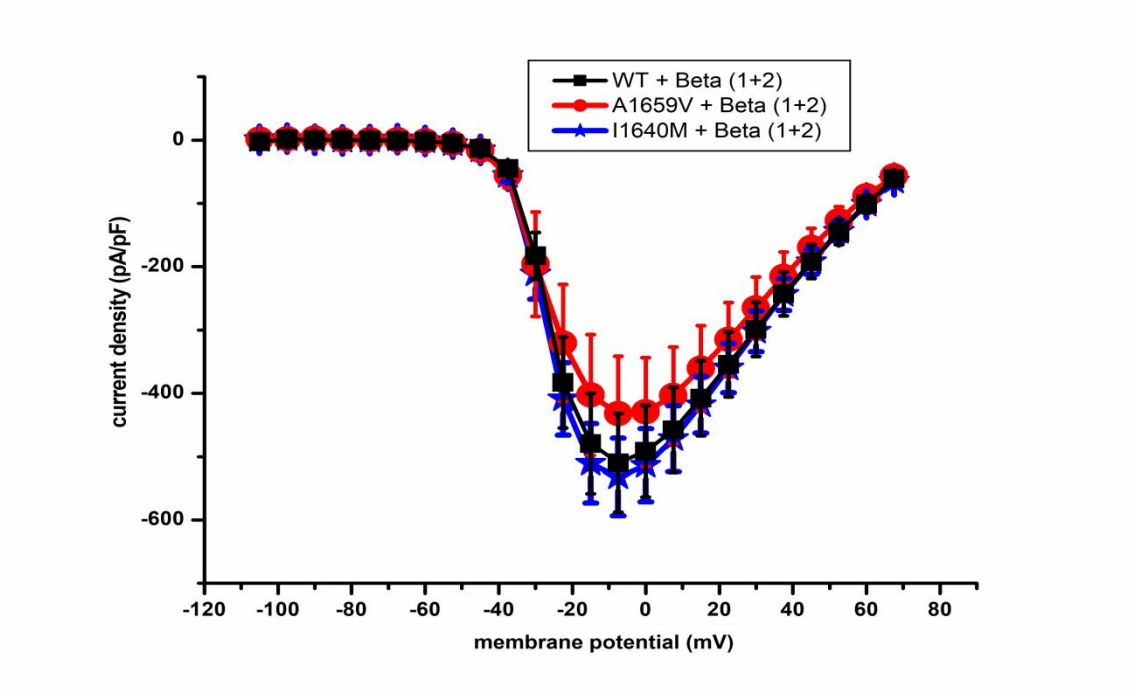

Figure 11: Current density.

The two mutants exhibited similar current density compared with WT. Black: WT; red: A1659V mutation; blue: I1640M mutation. Compare to table 6 for results.

The current density equals to peak current amplitude (pA)/capacitance (pF). The I1640M mutation and WT had a similarity current density. The A1659V-transfected tsA201 cells showed a slightly lower current density (-452.7 ± 95.5 pA/pF, Table 6) compared to the WT (-543.9 ± 62.4 pA/pF, Table 6), but no statistical difference compared to WT (Figure 11, Table 6).

Table 6. Current density.

Current density: current peak (pA)/capacitance (pF); n: cells number. WT: n=31; A1659V: n=15; I1640M: n=18. Mean ± SEM was used for data presentation. The P-value of Kruskal-Wallis ANOVA on ranks marked as $^{※}$: <0.05, $^{※※}$: <0.01, $^{※※※}$: <0.001.

	current density (pA/pF)	***n***
WT	-543.9 ± 62.4	31
A1659V	-452.7 ± 95.5	15
I1640M	-549.7 ± 74.4	18

3.3.3. Persistent current

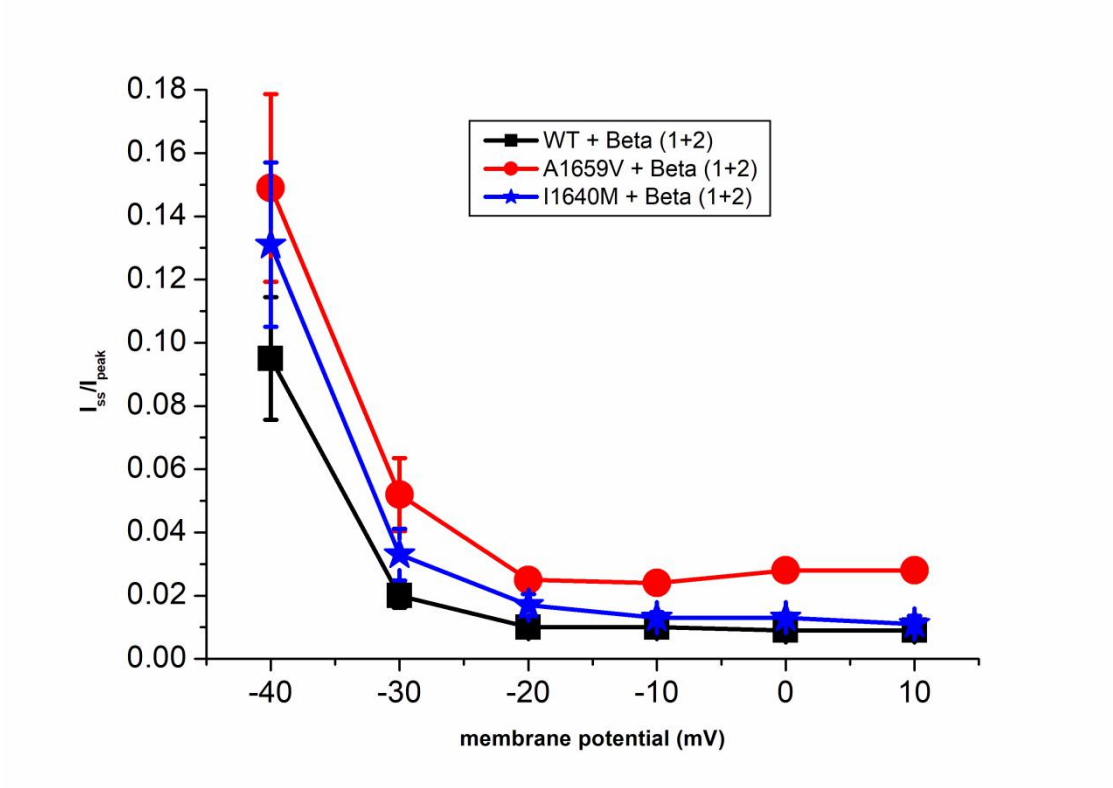

Figure 12: Persistent current.

The persistent currents, termed as I_{SS}/I_{Peak}. I_{SS}: the current amplitude； I_{Peak}: the maximum peak current. Black: WT; red: A1659V mutation; blue: I1640M mutation. Compare to table 7 for results.

The persistent currents, termed as I_{SS}/I_{Peak}. For the A1659V mutation, the persistent current was significantly increased compared to the WT (at -30 mV: A1659V: 5.190% ± 0.012 vs. WT: 2.000% ± 0.004, ※※P < 0.01; at -20 mV: A1659V: 2.490% ± 0.003 vs. WT: 1.020% ± 0.002, ※※※P < 0.001; at -10 mV: A1659V: 2.360% ± 0.002 vs. WT: 1.030% ± 0.001, ###P < 0.001; at 0 mV: A1659V: 2.810% ± 0.003 vs. WT: 0.929% ± 0.001, ※※※P < 0.001; at +10 mV: A1659V: 2.790% ± 0.003 vs. WT: 0.886% ± 0.001, ※※※P < 0.001; A1659V, *n* =14； WT， n=21, Figure 12, Table 7-A). The A1659V mutation caused a larger persistent sodium current (I_{Na}) than the WT (at -30, -20, -10, 0 and +10 mV). This increasing persistent I_{Na} meant that A1659V mutation increased the inward I_{Na} which could explain abnomal neuronal electrical activity. In

contrast, the persistent currents of the I1640M mutation had no statistical difference comparing with WT (Figure 12, Table 7-B).

Table 7. Persistent current.

I_{SS}/I_{Peak} (steady-state current/initial peak current): the persistent current (as mentioned above); n: cells number. The A1659V mutation (at -30, -20, -10, 0 and +10 mV) was significantly increased compared to WT. Mean ± SEM was used for data presentation. The P-value of One-way ANOVA marked as $^{\#}$: <0.05, $^{\#\#}$: <0.01, $^{\#\#\#}$: <0.001. Dunnet's test was used to correct multiple comparisons; The P-value of Kruskal-Wallis ANOVA on ranks marked as $^{※}$: <0.05, $^{※※}$: <0.01, $^{※※※}$: <0.001. Dunn's test was used to correct multiple comparisons.

A

V (m V)	WT		A1659V	
	I_{SS}/I_{Peak} (%)	***n***	**I_{SS}/I_{Peak} (%)**	***n***
-40	9.500% ± 0.019	21	14.900% ± 0.030	14
-30	2.000% ± 0.004	21	**5.190% ± 0.012**$^{※※}$	14
-20	1.020% ± 0.002	21	**2.490% ± 0.003**$^{※※※}$	14
-10	1.030% ± 0.001	21	**2.360% ± 0.002**$^{\#\#\#}$	14
0	0.929% ± 0.001	21	**2.810% ± 0.003**$^{※※※}$	14
+10	0.886% ± 0.001	21	**2.790% ± 0.003**$^{※※※}$	14

B

V (m V)	WT		I1640M	
	I_{SS}/I_{Peak} (%)	***n***	**I_{SS}/I_{Peak} (%)**	***n***
-40	9.500% ± 0.019	21	13.100% ± 0.026	17
-30	2.000% ± 0.004	21	3.250% ± 0.008	17
-20	1.020% ± 0.002	21	1.730% ± 0.004	17
-10	1.030% ± 0.001	21	1.350% ± 0.002	17
0	0.929% ± 0.001	21	1.330% ± 0.001	17
+10	0.886% ± 0.001	21	1.130% ± 0.003	17

3.3.4. Activation and fast inactivation curves

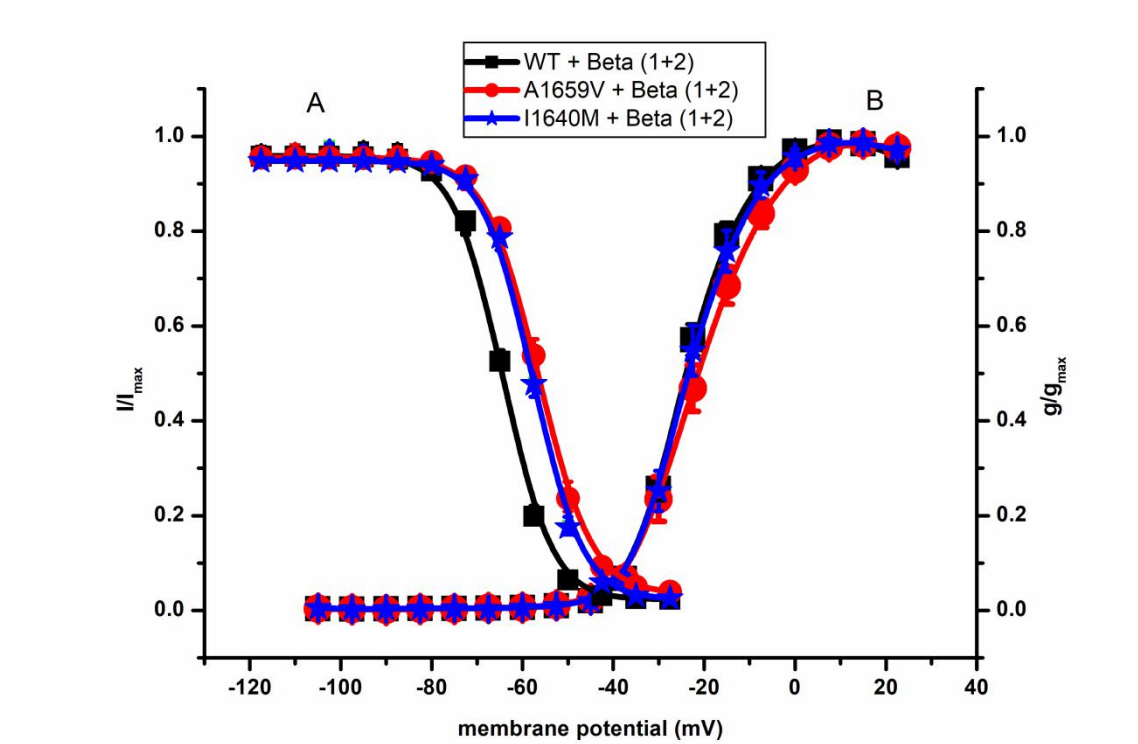

Figure 13: Fast inactivation (A) and activation curves (B).

Conductance-voltage (g-V) relationship was shown in the activation curves. The current amplitudes normalizing to the largest current amplitudes were shown in fast inactivation curves. The figure was fitted to Boltzmann function. The half-maximum inactivation voltage of two mutations significantly shifted (I1640M shifted by 7 mV and A1659V shifted by 8 mV) comparing to the WT. A: black: WT, n=30; red: A1659V mutation, n=15; blue: I1640M mutation, n=18. B: Black: WT, n=31; red: A1659V mutation, n=15; blue: I1640M mutation, n=18. Compare to table 8 and 9 for results.

The activation curve records the changes of the whole-cell peak current upon different step depolarizations and reflects the speed and ease of channel opening. For the activation curve (measured during voltage steps from -105 to +20 mV), defects caused by the A1659V mutation ($V_{1/2\ activ.}$ = -21.7 ± 1.4 mV, Figure 13-B, Table 8) showed a slight depolarizing shift compared to WT ($V_{1/2\ activ.}$ = -23.8 ± 0.9 mV, Figure 13-B, Table 8), but no statistical difference compared to the WT. The I1640M mutation also showed no statistical difference comparing to WT in the activation curve (Figure 13-B, Table 8). The slopes of activation curves of two mutations were no statistical differences compared to WT (Figure 13-B, Table 8).

Table 8. **The parameter of activation curves.**

$V_{1/2}$ activation: voltage of half-maximum activation; k: slope of activation curve; n: cells number. Mean ± SEM was used for data presentation.

	$V_{1/2}$ activation (mV)	**k**	***n***
WT	-23.8 ± 0.9	-5.1 ± 0.3	31
A1659V	-21.7 ± 1.4	-6.1 ± 0.4	15
I1640M	-23.1 ± 1.3	-5.2 ± 0.3	18

The fast inactivation curve demonstrated a significant 8 mV depolarizing shift for the A1659V mutation (A1659V: -56.5 ± 0.8 mV vs. WT: -64.3 ± 0.5 mV, A1659V: *n* =15, WT: n=30, $^{###}$P < 0.001, Figure 13-A, Table 9) compared to the WT. For the I1640M mutation, there was also a significant depolarizing shift of 7 mV (I1640M: -57.7 ± 0.6 mV vs. WT: -64.3 ± 0.5 mV, I1640M: *n* =18, WT: n=30, $^{###}$P < 0.001, Figure 13-A, Table 9) compared to the WT. The slopes of fast inactivation curves of two mutations were no statistical differences comparing to the WT (Figure 13-A, Table 9). This change (significant shift in depolarizing direction in fast inactivation curve) increased more available channels at a given membrane potential that could be activated for an action potential and therefore reflected another gain-of-function (GOF) effect.

Table 9. **The parameter of fast inactivation curves.**

$V_{1/2}$ inactivation: voltage of half-maximum fast inactivation; k: slope of fast inactivation curve; n: cells number. There was a significant difference between the two mutations and the WT in the $V_{1/2}$ inactivation. Mean ± SEM was used for data presentation. The P-value of One-way ANOVA marked as $^{#}$: <0.05, $^{##}$: <0.01, $^{###}$: <0.001. Dunnet's test was used to correct multiple comparisons.

	$V_{1/2}$ inactivation (mV)	**k**	***n***
WT	-64.3 ± 0.5	4.6 ± 0.1	30
A1659V	**-56.5 ± 0.8$^{###}$**	5.1 ± 0.2	15
I1640M	**-57.7 ± 0.6$^{###}$**	4.7 ± 0.2	18

3.3.5. The time constant and time course of recovery from fast inactivation

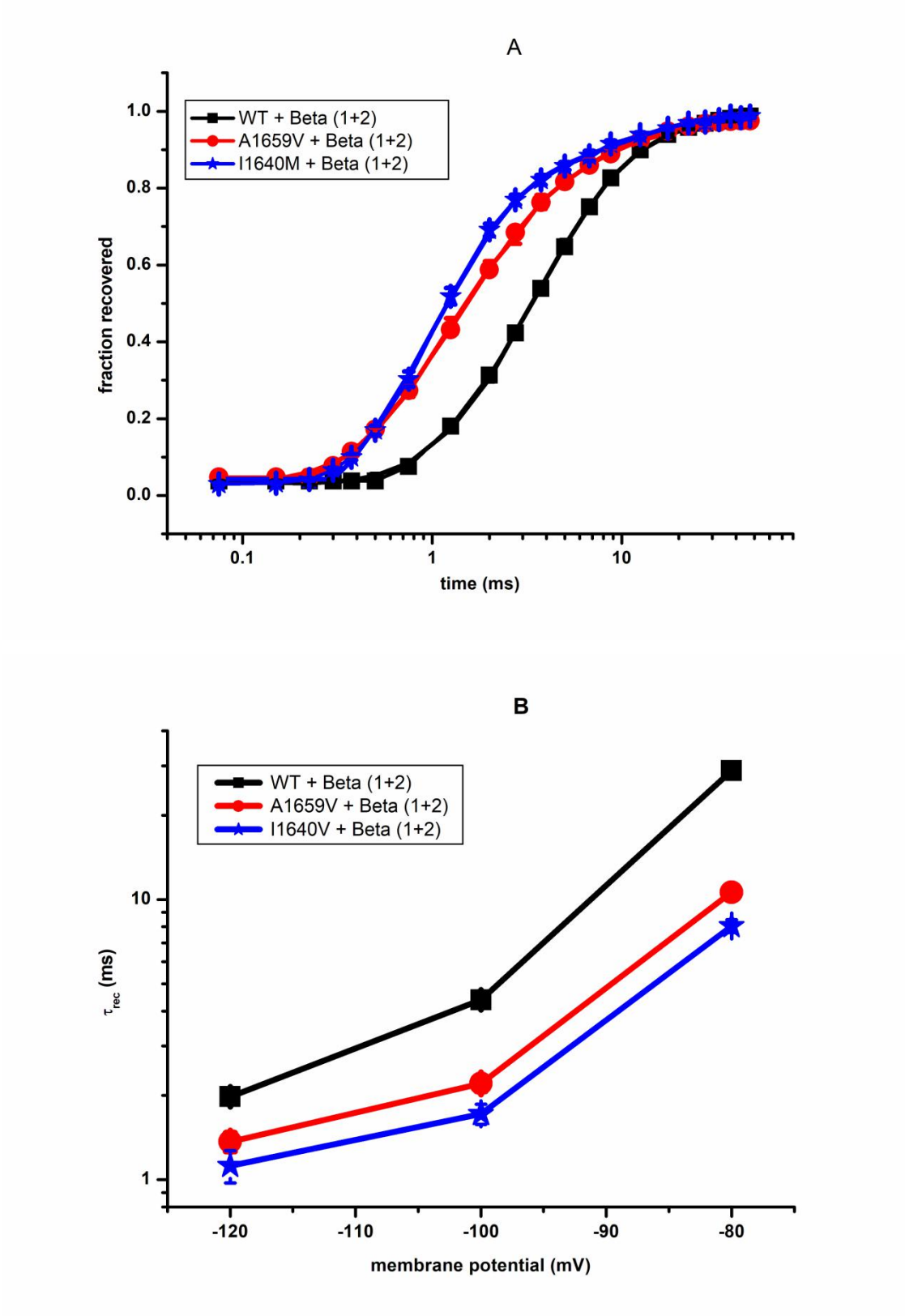

Figure 14: A: The time course of recovery from fast inactivation (at -100 mV); B: The time constant of recovery from fast inactivation. Compare to table 10 (A, B and C) for results.

At -80, -100 and -120 mV, the A1659V mutation showed a decreased time constant of recovery from fast inactivation comparing to WT ((at -80 mV) A1659V: 10.6 ± 0.7 ms vs. WT: 28.9 ± 1.5 ms, A1659V: n =15, WT: n=29, ※※※P < 0.001; (at -100 mV) A1659V: 2.2 ± 0.1 ms vs. WT: 4.4 ± 0.2 ms, A1659V: n =15, WT: n=30, ※※※P < 0.001; (at -120 mV) A1659V: 1.4 ± 0.1 ms vs. WT: 2.0 ± 0.1 ms, A1659V: n =15, WT: n=30, ※※※P < 0.001; Figure 14-A and B, Table 10-A, B and C).

The I1640M mutation also caused a decreased time constant of recovery from fast inactivation at -80, -100 and -120 mV comparing to the WT ((at -80 mV) I1640M: 8.0 ± 0.4 ms vs. WT: 28.9 ± 1.5 ms, I1640M: n =18, WT: n =29, ※※※P < 0.001; (at -100 mV) I1640M: 1.7 ± 0.1 ms vs. WT: 4.4 ± 0.2 ms, I1640M: n =17, WT: n =30, ※※※P < 0.001; (at -120 mV) I1640M: 1.1 ± 0.1 ms vs. WT: 2.0 ± 0.1 ms, I1640M: n =18, WT: n =30, ※※※P < 0.001; Figure 14-A and B, Table 10-A, B and C).

Table 10. The time constant of recovery from fast inactivation.

τ_{rec}: time constant of recovery from fast inactivation; n: cells number. Both I1640M and A1659V mutations accelerated the recovery from fast inactivation at -80 mV (A), -100 mV (B) and -120 mV (C) comparing to WT. Mean ± SEM was used for data presentation. The P-value of Kruskal-Wallis ANOVA on ranks marked as ※: <0.05, ※※: <0.01, ※※※: <0.001. Dunn's test was used to correct multiple comparisons.

A

	τ_{rec} (ms) at -80 mV	***n***
WT	28.9 ± 1.5	29
A1659V	**10.6 ± 0.7**※※※	15
I1640M	**8.0 ± 0.4**※※※	18

B

	τ_{rec}(ms) at -100 mV	***n***
WT	4.4 ± 0.2	30
A1659V	**2.2 ± 0.1**※※※	15
I1640M	**1.7 ± 0.1**※※※	17

C

	τ_{rec}(ms) at -120 mV	*n*
WT	2.0 ± 0.1	30
A1659V	**1.4 ± 0.1**※※※	15
I1640M	**1.1 ± 0.1**※※※	18

3.3.6. The time constant of fast inactivation

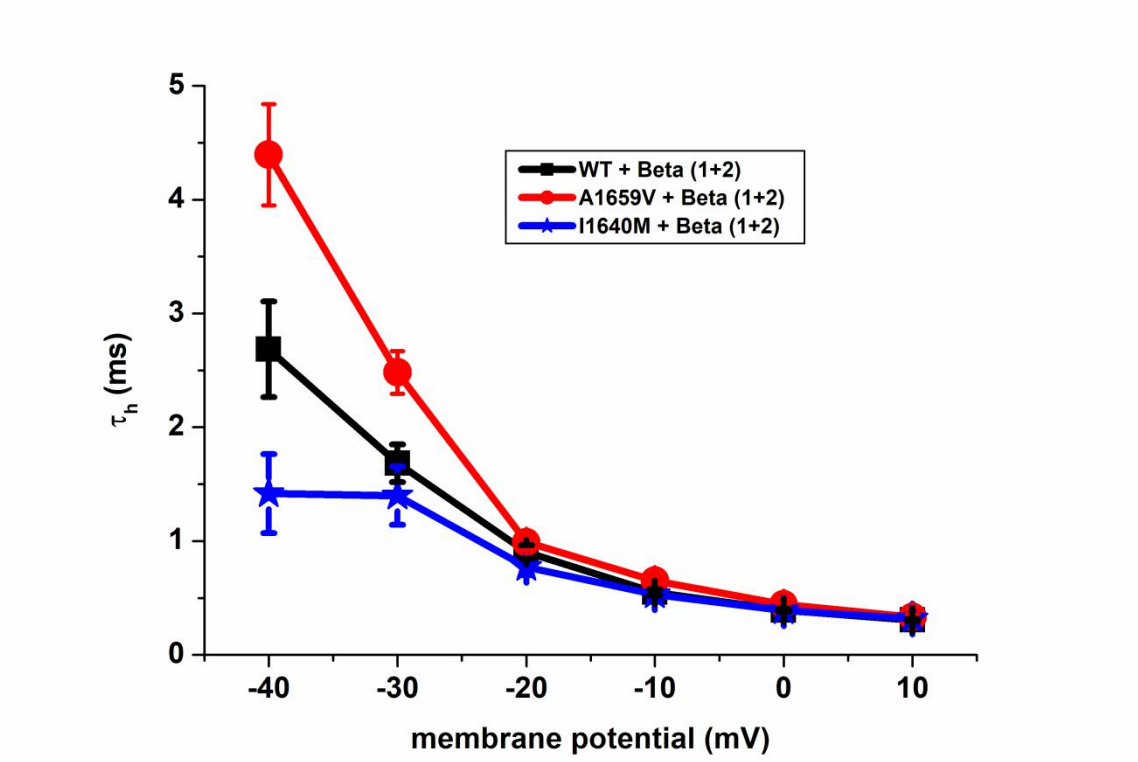

Figure 15: The time constant of fast inactivation.

Black: WT; red: A1659V mutation; blue: I1640M mutation. Compare to table 11 for results.

For the A1659V mutation, the time constant of fast inactivation at -40 mV was increased compared with the WT (A1659V: 4.40 ± 0.45 ms vs. WT: 2.69 ± 0.42 ms, ※P < 0.05, A1659V: *n* =14, WT: n=27; Figure 15, Table 11-A). Slowing of transition from activation to fast inactivation may increase the inward I_{Na}. The I1640M mutation of the fast inactivation time constant had no statistical difference compared to the WT (Figure 15, Table 11-B).

Table 11. The time constant of fast inactivation.

τ_h, time constant of fast inactivation; n: cells number. At -40 mV the A1659V mutation caused an increased time constant compared with the WT. Mean ± SEM was used for data presentation. The P-value of Kruskal-Wallis ANOVA on ranks marked as ※: <0.05, ※※: <0.01, ※※※: <0.001. Dunn's test was used to correct multiple comparisons.

A

V (m V)	WT		A1659V	
	τ_h (ms)	*n*	τ_h (ms)	*n*
-40	2.69 ± 0.42	27	**4.40 ± 0.45**※	14
-30	1.68 ± 0.17	31	2.48 ± 0.40	15
-20	0.90 ± 0.07	31	0.98 ± 0.07	15
-10	0.55 ± 0.03	31	0.65 ± 0.04	15
0	0.39 ± 0.01	31	0.44 ± 0.02	15
+10	0.31 ± 0.01	31	0.33 ± 0.02	15

B

V (m V)	WT		I1640M	
	τ_h (ms)	*n*	τ_h (ms)	*n*
-40	2.69 ± 0.42	27	1.42 ± 0.36	18
-30	1.68 ± 0.17	31	1.40 ± 0.25	18
-20	0.90 ± 0.07	31	0.77 ± 0.07	18
-10	0.55 ± 0.03	31	0.53 ± 0.04	18
0	0.39 ± 0.01	31	0.39 ± 0.02	18
+10	0.31 ± 0.01	31	0.32 ± 0.02	18

3.4 The functional consequences of the A1659V and I1640M mutations in $hNa_V1.2$

As mentioned above, the A1659V and I1640M mutations changed the kinetics and voltage-dependent characteristics of $hNa_V1.2$ in the transfected tsA201 cells (Table 12). For the A1659V mutation, which is located in the linker of DIV-S4-S5, caused the inactivation curve shifted 8 mV towards a depolarizing direction, a decreasing time constant at -80, -100 and -120 mV in the recovery from fast inactivation, an increasing persistent I_{Na} at -30, -20, -10, 0 and +10 mV, and a longer time constant at -40 mV in fast inactivation. The I1640M mutation, which locates in the DIV-S4, shifted 7 mV in depolarizing direction in fast inactivation and also decreased time constant of recovery from fast inactivation at -80, -100 and -120 mV. Neither A1659V nor I1640M mutation showed a statistical difference comparing to WT in the activation curve and current density.

Table 12. The electrophysiological characteristics of A1659V and I1640M mutations in $hNa_V1.2$.

Both of the A1659V and I1640M mutations in transfected tsA201 cells affected different parameters of fast inactivation of $hNa_V1.2$ but did not significantly change parameters of activation.

Functional analyses	The A1659V mutation	The I1640M mutation
$V_{1/2}$ of fast inactivation curve	depolarizing shift	depolarizing shift
The time constant of recovery from fast inactivation (at -80,-100 and -120 mV)	decreased	decreased
Persistent current (at -30, -20, -10, 0 and +10 mV)	increased	-
The time constant of fast inactivation (at -40 mV)	increased	-
Current density	-	-
Activation curve	-	-

4. Discussion

The hNa$_V$1.2 is encoded by *SCN2A* and composed of 2005 amino acid residues. hNa$_V$ 1.2 is mainly distributed in the human brain, and the phenotype spectrum of mutations in *SCN2A* include BFNIS, GEFS+ and EE (Brunklaus et al., 2014). Previous studies have shown *SCN2A* mutations GOF effect alongside a depolarizing shift in inactivation curve, an increasing sodium current density, shifting in hyperpolarizing direction in activation curve, or acceleration recovery from fast inactivation, as well as loss-of-function (LOF) effect alongside shifting in depolarizing direction in activation curve, shifting in hyperpolarizing direction in inactivation curve or a prolonging recovery from fast inactivation (Schwarz et al., 2016, Wolff et al., 2017).

This dissertation provided the functional studies of two additional neonatal-onset epilepsy-associated *SCN2A* mutations. The results presented in this thesis that these two mutations associated with neonatal-onset epilepsy caused different GOF effects in hNa$_V$1.2.

4.1. The functional consequences of two neonatal-onset epilepsy-associated *SCN2A* mutations

4.1.1. The I1640M mutation affected the hNa$_V$1.2 fast inactivation not activation process

In this thesis, we performed functional studies in tsA201 cells co-expressing hNa$_V$1.2 WT or mutants and auxiliary hβ1 and hβ2-subunits by using electrophysiology technique (as mentioned above). The I1640M mutation locates in DIV-S4 of hNa$_V$1.2. Previous studies showed that DIV-S4 mutations altered fast inactivation process (Chanda et al., 2004). This thesis presented in fast inactivation curve the I1640M mutation shifted 7 mV in depolarizing direction. This change indicated that this DIV-S4 mutation affected the fast inactivation process. In contrast, there were no significant changes in the I1640M mutation in the activation curve.

On the basis of earlier studies, DIV-S4 affected more in fast inactivation than in the activation process, whereas the DI-S4 and DII-S4 affected activation process (Lerche et al., 1996, Cha et al., 1999). The S4 segment is unequally charged in different domains (Chen et al., 1996) which may explain why the S4 segments play different roles in activation and fast inactivation process in different domains (Kontis and Goldin, 1997).

4.1.2. The A1659V mutation affected the hNa$_V$1.2 different parameters of the fast inactivation process

Previous studies showed that the mutations in DIV-S4-S5 affected fast inactivation (Popa et al., 2004). This thesis showed that the A1659V mutation, which locates in DIV-S4-S5, in fast inactivation curve shifted 8 mV in depolarizing direction, increased persistent I_{Na}, slowed to fast inactivation and accelerated recovery from fast inactivation. All mentioned above indicated that inactivation state was severely destabilized by this mutation which corroborated the findings presented in previous studies.

4.1.3. The I1640M and A1659V mutations both affected the process of fast inactivation

After an action potential, the channel has no response to the potential change, this process is called refractory period. This period is affected by recovery from fast inactivation; whereas fast inactivation time constants indicate the decay of current after a depolarization. This thesis presented that the two mutations accelerated recovery from fast inactivation, which meant cutting down the refractory period. This functional study also showed a larger persistent I_{Na} and a slowing fast inactivation for A1659V mutation. A slower fast inactivation and increasing persistent I_{Na} implied an increase in the inward movement of sodium ions (for the A1659V mutation). Moreover, the depolarizing shift of these two mutations in fast inactivation curve indicated more channels available for the opening during the process of the action potential.

All these alterations indicated that two mutations caused different GOF defects in hNa$_V$1.2. Therefore, it can be hypothesized that the functional effect caused by the two

mutations may induce a neuronal hyperexcitability which can lead to seizures in neonatal-onset epilepsy.

4.1.4. Functional studies for epilepsy-associated *SCN2A* mutations

Many epilepsy-associated *SCN2A* mutations have been reported previously, but only some of them have been functionally studied (Liao et al., 2010a, Liao et al., 2010b, Lauxmann et al., 2013, Schwarz et al., 2016, Wolff et al., 2017). The phenotypic spectrum of these mutations ranges from mild BFNIS to severe EE (Table 13). The mutations of severe epilepsy syndrome tend to emerge *de novo*. The relationship between genotype and phenotype in GOF mutations has not been entirely clear until now, with different mutations resulting in same phenotype and the same mutation causing various phenotypes (a phenomenon known as pleiotropy). However, as can be seen here for the two mutations causing relatively severe phenotypes, in particular for the A1659V mutation, the severity of the phenotype seems to correlate in part with the severity of the electrophysiological changes, which were usually milder in cases causing BFNIS. Other members of our lab have recently confirmed this by comparing clinical and electrophysiological *in vitro* phenotypes of all mutations published so far (Lauxmann et al., submitted). The results presented here, fit into this scheme. However, due to the pleiotropy, the unknown genetic background factors must be considered to explain phenotypic variability besides the direct effects of the mutations. In addition to GOF changes, many LOF changes have been described (for references see Table 13). Wolff et al. (2017) recently established the relationship between the onset of disease and GOF/LOF changes. They showed that GOF mutations were associated with early-onset (earlier than three months in life) whereas LOF mutations were related to late-onset.

Table 13. The functional studies of mutations in *SCN2A* associated with epilepsy, revised from (Wolff et al., 2017).

BFNIS: Benign familial neonatal-infantile seizures, BFNS: Benign familial neonatal seizures, BNS: Benign neonatal seizures, d: day(s), DS: Dravet syndrome, EE: Epileptic encephalopathy, EIMFS: Epilepsy of infancy with migrating focal seizures, EOEE: Early onset epileptic encephalopathy, FS: Febrile seizures, GOF: gain-of-function, IS: Infantile spasms, LOF: loss-of-function, m: month(s), LGS: Lennox-Gastaut syndrome, MAE: Myoclonic-atonic epilepsy, OS: Ohtahara syndrome, TCS: Tonic-clonic seizure, w: week(s), y: year(s).

Mutations/inheritance	First seizure onset	Phenotype or type of seizure	Functional change	Published in
V423L / *de novo*	1d, 6d	OS	GOF	Wolff et al., 2017
F1597L / *de novo*	3d	EIMFS	GOF	Wolff et al., 2017
P1622S / *de novo*	21m	MAE	LOF	Wolff et al., 2017
V261M / *de novo*	1d	BFNS	GOF	Liao et al. 2010
M252V / maternal	4m	BFNIS	GOF	Liao et al. 2010
R1882G / *de novo*	2d	BIS	GOF	Schwarz et al. 2016
A263V / *de novo*	1d-3w	BNS, OS, EE	GOF	Schwarz et al. 2016 Johannesen et al. 2016 Touma et al. 2013 Wolff et al., 2017 Liao et al. 2010
Y1589C / familial	3m	BFIS	GOF	Lauxmann et al. 2013
R1319Q / maternal	3m	BFIS	LOF+GOF	Scalmani et al, 2006 Misra et al. 2008
L1330F / familial	6w	BFIS	LOF GOF	Misra et al. 2008 Scalmani et al, 2006
L1563V / familial	3m	BFIS	GOF LOF	Misra et al. 2008 Scalmani et al, 2006 Xu et al. 2007 Misra et al. 2008
R102X / *de novo*	19m	EE	LOF	Kamiya et al. 2004
E1211K / *de novo*	11m	IS	LOF+GOF	Ogiwara et al. 2009
I1473M / *de novo*	1m	EE	GOF	Ogiwara et al. 2009

R223Q / familial	3m	BFNIS	GOF	Scalmani et al. 2006
A263T / *de novo*	3d	EOEE	GOF	Nakamura et al. 2013
R188W / paternal	8m	FS	GOF	Sugawara et al. 2001
E717G* fs / *de novo*	3y	EE	LOF	Horvath et al. 2016
I1021Y* fs / *de novo*	N/A, 14m	LGS, EE	LOF	Carvill et al. 2013 Howell et al. 2015
R1312T / unknown	11m	DS	LOF	Shi et al. 2009
R1435X / *de novo*	3y	Epilepsy	LOF	Trump et al. 2016

4.2. The relationship between human VGSC mutations and treatment response to AEDs

VGSCs are the targets of the sodium channel blockers, which are first-line AEDs that stabilize the inactivation process of VGSCs thereby preventing high frequency neuronal activating and reducing the number of action potentials (https://learn.pharmacy.unc.edu/) (Depondt, 2006). Previous studies showed that sodium ion channel gene mutations may be associated with response to AEDs treatment.

The research on response to AEDs treatment and discovering new AEDs has become the focus of clinicians' concerns. Until now, there have been few studies focusing on the relationship between the mutations of VGSC genes and the response to AEDs treatment. One functional study about a mutation of *SCN1B* associated with GEFS+ showed that this mutation reduced the channel sensitivity to phenytoin, and it revealed that the mutation could alter the response to AEDs as a result of channel gating function changes (Lucas et al., 2005). Another previous study reported that defects in the functions of VGSCs were a potential factor resistant to AEDs (Jang et al., 2009). Wolff et al. (2017) showed functional characterization changes could predict the response to the AEDs treatment and that GOF made a good response to sodium channel blockers, whereas LOF showed an insufficient response (Wolff et al., 2017).

As mentioned above, the epileptic phenotype associated with different mutations showed different responses to AEDs treatment. This indicates that it is crucial for clinicians to make individualized therapy plans for epilepsy patients. According to results presented here, the carriers of the two mutations investigated in this thesis should respond well to sodium blockers.

5. Summary

Human brain VGSCs are related to the action potential of the neuron. Functional changes happen in human VGSCs can induce neuronal hyperexcitability and result in seizures. *SCN2A* which codes for the $hNa_v1.2$ channel, is one important gene associated with neonatal-onset epilepsy. Neonatal-onset epilepsy is defined as an onset within four weeks after birth. A severe neonatal-onset epilepsy can cause permanent developmental regression and resistance to AEDs treatment.

In this dissertation, both A1659V and I1640M mutations of *SCN2A* associated with neonatal-onset epilepsy were functionally analyzed using electrophysiology technique. Either the WT or the mutation, with the hβ1 and hβ2, were co-expressed in tsA201 cells for functional studies. Both mutations shifted in depolarization direction in fast inactivation and speed up recovery from it. Moreover, A1659V mutation presented increasing persistent I_{Na} and slower fast inactivation. All these functional changes indicated clear GOF effects. These functional consequences predict an increase in channel availability for action potentials, a shorter refractory period and more inward sodium current that can depolarize the neuronal cell membrane. The detected changes can therefore well explain a neuronal hyperexcitability which can result in epileptic seizures.

Further studies need to be performed using neurons and neuronal networks to understand neuronal hyperexcitability. First consequences for treatment result from such studies since GOF mutations in *SCN2A* can be well treated by Na^+ channel blockers. However, further drugs are needed, since not all patients respond and some have severe side effects.

6. Zusammenfassung

Für die Depolarisation bei einem Aktionspotential von Nervenzellen im menschlichen Gehirn sind in erste Linie spannungsabhängige Natriumkanäle (Na_V) verantwortlich. Funktionelle Veränderungen in diesen Kanälen können eine neuronale Übererregbarkeit verursachen und dadurch Anfälle auslösen. *SCN2A*, welches für den spannungsabhängigen Natriumkanal $hNa_V1.2$ kodiert, ist ein wichtiges Gen welches mit neonatalen Epilepsien assoziiert ist. Neonatale Epilepsien sind durch das erstmalige Auftreten eines Anfalls in den ersten vier Wochen nach der Geburt definiert. Schwere neonatale Epilepsien können zu Entwicklungsrückschritten führen und sind oft therapierefraktär.

In dieser Dissertation wurden die beiden *SCN2A* Mutationen A1659V und I1640M mit Hilfe der elektrophysiologische technik untersucht, welche beide neonatale Epilepsien verursachen. Für funktionelle Untersuchungen wurden entweder der Wildtyp oder eine der Mutationen zusammen mit den Untereinheiten hβ1 und hβ2 in tsA201 Zellen transfiziert. Beide Mutationen verursachen eine depolsarisierende Verschiebung bei der spannungsabhängigen Inaktivierung aus einem Gleichgewichtszustand und zusätzlich eine beschleunigte Erholung von der schnellen Inaktivierung. Zusätzlich zeigt die A1659V Mutation einen größeren persistierenden Strom und eine Verlangsamung der Zeitkonstante der schnellen Inaktivierung. All diese funktionellen Veränderungen deuten auf einen klaren Funktionszugewinn hin. Diese funktionellen Veränderungen weisen auf eine erhöhte Verfügbarkeit der Kanäle für ein Aktionspotential hin, sowie einer verkürzen Erholungsphase nach einem Aktionspotential und einem vergrößertem Natrium-Einwärts-Strom, welcher zu einer Depolarisation der neuronalen Zellmembran führen kann. Die gefunden Veränderungen können daher sehr gut eine neuronale Übererregbarkeit erklären, was epileptischen Anfällen verursachen kann.

Weitere Untersuchungen in Neuronen und neuronalen Netzwerken müssen durchgeführt werden, um eine Übererregbarkeit zu bestätigen. Erste Konsequenzen für die Behandlung ergeben sich aus solchen Studien, da Mutationen mit Funktionszugewinn in *SCN2A* gut mit Na-Kanal-Blockern behandelt werden können. Dennoch werden weitere

Medikamente benötigt, da nicht alle Patienten auf die Behandlung ansprechen und einige unter schweren Nebeneffekten leiden.

7. References

BRUNKLAUS, A., ELLIS, R., et al. 2014. Genotype phenotype associations across the voltage-gated sodium channel family. *J Med Genet,* 51**,** 650-8.

BRUNKLAUS, A. & ZUBERI, S. M. 2014. Dravet syndrome--from epileptic encephalopathy to channelopathy. *Epilepsia,* 55**,** 979-84.

CATTERALL, W. A. 1992. Cellular and molecular biology of voltage-gated sodium channels. *Physiol Rev,* 72**,** S15-48.

CATTERALL, W. A. 2000. From ionic currents to molecular mechanisms: the structure and function of voltage-gated sodium channels. *Neuron,* 26**,** 13-25.

CATTERALL, W. A. 2001. A 3D view of sodium channels. *Nature,* 409**,** 988-9, 991.

CATTERALL, W. A. 2014. Sodium channels, inherited epilepsy, and antiepileptic drugs. *Annu Rev Pharmacol Toxicol,* 54**,** 317-38.

CHA, A., RUBEN, P. C., et al. 1999. Voltage sensors in domains III and IV, but not I and II, are immobilized by Na+ channel fast inactivation. *Neuron,* 22**,** 73-87.

CHANDA, B., ASAMOAH, O. K., et al. 2004. Coupling interactions between voltage sensors of the sodium channel as revealed by site-specific measurements. *J Gen Physiol,* 123**,** 217-30.

CHEN, L. Q., SANTARELLI, V., et al. 1996. A unique role for the S4 segment of domain 4 in the inactivation of sodium channels. *J Gen Physiol,* 108**,** 549-56.

COPPOLA, G., PLOUIN, P., et al. 1995. Migrating partial seizures in infancy: a malignant disorder with developmental arrest. *Epilepsia,* 36**,** 1017-24.

COVANIS, A. 2012. Epileptic encephalopathies (including severe epilepsy syndromes). *Epilepsia,* 53 Suppl 4**,** 114-26.

DEPONDT, C. 2006. The potential of pharmacogenetics in the treatment of epilepsy. *Eur J Paediatr Neurol,* 10**,** 57-65.

ENGEL, J., JR. 2006. Report of the ILAE classification core group. *Epilepsia,* 47**,** 1558-68.

ENGEL, J., JR. & INTERNATIONAL LEAGUE AGAINST, E. 2001. A proposed diagnostic scheme for people with epileptic seizures and with epilepsy: report of the ILAE Task Force on Classification and Terminology. *Epilepsia,* 42**,** 796-803.

EPI4K, C., EPILEPSY PHENOME/GENOME, P., et al. 2013. De novo mutations in epileptic encephalopathies. *Nature,* 501**,** 217-21.

ERIC R. KANDEL, J. H. S., THOMAS M. JESSELL 2000. *Principles of Neural Science 4th_Edition*.

FISHER, R. S. 2017. The New Classification of Seizures by the International League Against Epilepsy 2017. *Curr Neurol Neurosci Rep,* 17**,** 48.

GARDINER, M. 2006. Molecular genetics of infantile nervous system channelopathies. *Early Hum Dev,* 82**,** 775-9.

GOKBEN, S., ONAY, H., et al. 2017. Targeted next generation sequencing: the diagnostic value in early-onset epileptic encephalopathy. *Acta Neurol Belg,* 117**,** 131-138.

HOWELL, K. B., MCMAHON, J. M., et al. 2015. SCN2A encephalopathy: A major cause of epilepsy of infancy with migrating focal seizures. *Neurology,* 85**,** 958-66.

ISOM, L. L. 2001. Sodium channel beta subunits: anything but auxiliary. *Neuroscientist,* 7**,** 42-54.

ISOM, L. L., DE JONGH, K. S., et al. 1992. Primary structure and functional expression of the beta 1 subunit of the rat brain sodium channel. *Science,* 256**,** 839-42.

ISOM, L. L., RAGSDALE, D. S., et al. 1995. Structure and function of the beta 2 subunit of brain sodium channels, a transmembrane glycoprotein with a CAM motif. *Cell,* 83**,** 433-42.

ITO, M., NAGAFUJI, H., et al. 2002. Autosomal dominant epilepsy with febrile seizures plus with missense mutations of the (Na+)-channel alpha 1 subunit gene, SCN1A. *Epilepsy Res,* 48**,** 15-23.

JANG, S. Y., KIM, M. K., et al. 2009. Gene-to-gene interaction between sodium channel-related genes in determining the risk of antiepileptic drug resistance. *J Korean Med Sci,* 24**,** 62-8.

KAMIYA, K., KANEDA, M., et al. 2004. A nonsense mutation of the sodium channel gene SCN2A in a patient with intractable epilepsy and mental decline. *J Neurosci,* 24**,** 2690-8.

KAPLAN, D. I., ISOM, L. L., et al. 2016. Role of Sodium Channels in Epilepsy. *Cold Spring Harb Perspect Med,* 6.

KHAN, S. & AL BARADIE, R. 2012. Epileptic encephalopathies: an overview. *Epilepsy Res Treat,* 2012**,** 403592.

KONTIS, K. J. & GOLDIN, A. L. 1997. Sodium channel inactivation is altered by substitution of voltage sensor positive charges. *J Gen Physiol,* 110**,** 403-13.

LAUXMANN, S., BOUTRY-KRYZA, N., et al. 2013. An SCN2A mutation in a family with infantile seizures from Madagascar reveals an increased subthreshold Na(+) current. *Epilepsia,* 54**,** e117-21.

LERCHE, H., MITROVIC, N., et al. 1996. Paramyotonia congenita: the R1448P Na+ channel mutation in adult human skeletal muscle. *Ann Neurol,* 39**,** 599-608.

LERCHE, H., SHAH, M., et al. 2013. Ion channels in genetic and acquired forms of epilepsy. *J Physiol,* 591**,** 753-64.

LIAO, Y., ANTTONEN, A. K., et al. 2010a. SCN2A mutation associated with neonatal epilepsy, late-onset episodic ataxia, myoclonus, and pain. *Neurology,* 75**,** 1454-8.

LIAO, Y., DEPREZ, L., et al. 2010b. Molecular correlates of age-dependent seizures in an inherited neonatal-infantile epilepsy. *Brain,* 133**,** 1403-14.

LOSSIN, C., WANG, D. W., et al. 2002. Molecular basis of an inherited epilepsy. *Neuron,* 34**,** 877-84.

LUCAS, P. T., MEADOWS, L. S., et al. 2005. An epilepsy mutation in the beta1 subunit of the voltage-gated sodium channel results in reduced channel sensitivity to phenytoin. *Epilepsy Res,* 64**,** 77-84.

MAGIORKINIS, E., SIDIROPOULOU, K., et al. 2010. Hallmarks in the history of epilepsy: epilepsy in antiquity. *Epilepsy Behav,* 17**,** 103-8.

MEISLER, M. H., O'BRIEN, J. E., et al. 2010. Sodium channel gene family: epilepsy mutations, gene interactions and modifier effects. *J Physiol,* 588**,** 1841-8.

MOLLEMAN, A. 2002. *Patch Clamping: An Introductory Guide To Patch Clamp Electrophysiology*.

O'MALLEY, H. A. & ISOM, L. L. 2015. Sodium channel beta subunits: emerging targets in channelopathies. *Annu Rev Physiol,* 77**,** 481-504.

OGIWARA, I., ITO, K., et al. 2009. De novo mutations of voltage-gated sodium channel alphaII gene SCN2A in intractable epilepsies. *Neurology,* 73**,** 1046-53.

ORSINI, A., ZARA, F., et al. 2017. Recent advances in epilepsy genetics. *Neurosci Lett*.

PATINO, G. A. & ISOM, L. L. 2010. Electrophysiology and beyond: multiple roles of Na+ channel beta subunits in development and disease. *Neurosci Lett,* 486**,** 53-9.

POPA, M. O., ALEKOV, A. K., et al. 2004. Cooperative effect of S4-S5 loops in domains D3 and D4 on fast inactivation of the Na+ channel. *J Physiol,* 561**,** 39-51.

PORYO, M., CLASEN, O., et al. 2017. Dravet syndrome: a new causative SCN1A mutation? *Clin Case Rep,* 5**,** 613-615.

SAMANTA, D. & RAMAKRISHNAIAH, R. 2015. De novo R853Q mutation of SCN2A gene and West syndrome. *Acta Neurol Belg,* 115**,** 773-6.

SATO, C., UENO, Y., et al. 2001. The voltage-sensitive sodium channel is a bell-shaped molecule with several cavities. *Nature,* 409**,** 1047-51.

SCHEFFER, I. E., BERKOVIC, S., et al. 2017. ILAE classification of the epilepsies: Position paper of the ILAE Commission for Classification and Terminology. *Epilepsia,* 58**,** 512-521.

SCHWARZ, N., HAHN, A., et al. 2016. Mutations in the sodium channel gene SCN2A cause neonatal epilepsy with late-onset episodic ataxia. *J Neurol,* 263**,** 334-43.

SHEN, H., ZHOU, Q., et al. 2017. Structure of a eukaryotic voltage-gated sodium channel at near-atomic resolution. *Science,* 355.

SHI, X., YASUMOTO, S., et al. 2012. Clinical spectrum of SCN2A mutations. *Brain Dev,* 34**,** 541-5.

SHI, X., YASUMOTO, S., et al. 2009. Missense mutation of the sodium channel gene SCN2A causes Dravet syndrome. *Brain Dev,* 31**,** 758-62.

STRIANO, P., BORDO, L., et al. 2006. A novel SCN2A mutation in family with benign familial infantile seizures. *Epilepsia,* 47**,** 218-20.

STUHMER, W., CONTI, F., et al. 1989. Structural parts involved in activation and inactivation of the sodium channel. *Nature,* 339**,** 597-603.

SYRBE, S., ZHOROV, B. S., et al. 2016. Phenotypic Variability from Benign Infantile Epilepsy to Ohtahara Syndrome Associated with a Novel Mutation in SCN2A. *Mol Syndromol,* 7**,** 182-188.

VENKATACHALAN, S. P., BUSHMAN, J. D., et al. 2007. Optimized expression vector for ion channel studies in Xenopus oocytes and mammalian cells using alfalfa mosaic virus. *Pflugers Arch,* 454**,** 155-63.

WANG, J. W., SHI, X. Y., et al. 2012. Prevalence of SCN1A mutations in children with suspected Dravet syndrome and intractable childhood epilepsy. *Epilepsy Res,* 102**,** 195-200.

WATANABE, E., FUJIKAWA, A., et al. 2000. Nav2/NaG channel is involved in control of salt-intake behavior in the CNS. *J Neurosci,* 20**,** 7743-51.

WILMSHURST, J. M., GAILLARD, W. D., et al. 2015. Summary of recommendations for the management of infantile seizures: Task Force Report for the ILAE Commission of Pediatrics. *Epilepsia,* 56**,** 1185-97.

WOLFF, M., JOHANNESEN, K. M., et al. 2017. Genetic and phenotypic heterogeneity suggest therapeutic implications in SCN2A-related disorders. *Brain,* 10.1093/brain/awx054.

YALLAPU, M. M., JAGGI, M., et al. 2012. Curcumin nanoformulations: a future nanomedicine for cancer. *Drug Discov Today,* 17**,** 71-80.

8. Declaration of contributions to the dissertation

The dissertation work was carried out at the Hertie Institute for Clinical Brain Research (HIH) under the supervision of Prof. Dr. Holger Lerche.

The study was designed by the group of Prof. Dr. Holger Lerche in cooperation with the collaborators Prof. Rima Nabbout in Paris and Prof. Maria Roberta Cilio in San Francisco.

After training by laboratory members Dr. Yuanyuan Liu and Dr. Ulrike Hedrich-Klimosch, I carried out all experiments independently.

Statistical analysis was carried out independently by myself (under the supervision of Dr. Yuanyuan Liu).

I confirm that I wrote the manuscript myself (under the supervision of Prof. Dr. Holger Lerche) and that any additional sources of information have been duly cited.

Signed_____

On _____ in Tübingen

9. Acknowledgment

This dissertation was completed under the guidance of my supervisor Prof. Dr. Holger Lerche who has profound knowledge, rigorous attitude and patient guidance. Here I would like to express my sincere thanks to Prof. Dr. Holger Lerche. Thank you for all of your support, encouragement and help for me in the past three years.

Thanks to the hospital which I worked in my motherland for supporting me to study in Germany.

I am very grateful to Dr. Yuanyuan Liu for teaching me the patch-clamp technique and data analysis.

Thanks to Dr. Ulrike Hedrich-Klimosch for being always ready for help during research and thesis writing.

My thanks go out to MD. Niklas Schwarz who helped me a lot during the patch clamp recording and thesis writing.

I am also grateful to everyone in the laboratory. Thanks for all your help!

Sincerely thank my parents, brother and friends for supporting me.

At last, thanks to myself never giving up when I face any obstacles!